Eur. Phys. J. Plus (2021) 136:698
https://doi.org/10.1140/epjp/s13360-021-01693-5

THE EUROPEAN PHYSICAL JOURNAL PLUS

Regular Article

Adaptive denoising for strong noisy images by using positive effects of noise

Mengen Shen[1], Jianhua Yang[1,a], Miguel A. F. Sanjuán[2,3], Yuqiao Zheng[4], Houguang Liu[1]

[1] Jiangsu Key Laboratory of Mine Mechanical and Electrical Equipment, School of Mechatronic Engineering, China University of Mining and Technology, Xuzhou 221116, Jiangsu, People's Republic of China
[2] Nonlinear Dynamics, Chaos and Complex Systems Group, Departamento de Física, Universidad Rey Juan Carlos, Tulipán s/n, 28933 Móstoles, Madrid, Spain
[3] Department of Applied Informatics, Kaunas University of Technology, Studentu 50-407, 51368 Kaunas, Lithuania
[4] School of Mechanical and Electronic Engineering, Lanzhou University of Technology, Lanzhou 730050, People's Republic of China

Received: 31 March 2021 / Accepted: 22 June 2021

Abstract Image denoising is the key step for image preprocessing. In particular, denoising of a strong noisy image is truly necessary, even though it might be difficult. Among the different image denoising methods, stochastic resonance (SR) has the advantage of using the constructive role of noise. However, a traditional bistable system cannot take full advantage of SR. To improve the performance of image denoising by using SR, we use a nonlinear system with a periodic potential to utilize the benefit of noise to a greater extent. Besides, adaptive processing is realized by an optimization algorithm. Compared to the image denoising method by SR in a bistable system, the method by SR in a nonlinear system with a periodic potential (PSR) is much more effective possessing a higher peak signal-to-noise ratio and less computation time. Further, the image denoising method by PSR is also superior to other common methods such as arithmetic mean filter, geometric mean filter, median filter and Wiener filter. The PSR method is effective in removing different types of noise present in images, such as gamma noise, uniform noise, Rayleigh noise, and exponential noise.

1 Introduction

Digital images are common information carriers in human social and industrial activities. However, during the process of imaging, compression and transmission, images are usually polluted by various types of noise [1, 2]. The inevitable noisy image, especially with a strong noise, is usually annoying because it hinders the understanding of image information. For a better understanding and obtaining a detailed information of the image, noisy images must be denoised [3].

Image denoising has been attracting much attention in the past few years [4, 5]. There are numerous methods that have been proposed so far. Some of the common methods are

[a] e-mail: jianhuayang@cumt.edu.cn (corresponding author)

smoothly filtered in the spatial domain. Among them, median filtering [6] and Wiener filtering [7] are based on a local neighborhood information of images, while non-local means here that the method is based on the whole image [8]. There are also some common methods of denoising in the transform domain [9], such as Fourier transform [10], discrete cosine transform [11] and wavelet transform [12]. Besides, the block-matching 3D method is proposed, which combines the idea of a spatial domain and a transform domain [13]. The method based on compressed sensing, which utilizes the prior knowledge of the sparsity difference between images and noise is used in [14]. In addition, a number of methods based on data-driven or model-driven deep learning have been used by researchers [15–17]. Although most of the above methods have a good performance, they mainly focus on eliminating rather than utilizing noise. Unfortunately, detail information might also be removed when they eliminate the noise of the image [18–20]. Furthermore, as the noise intensity increases, their denoising effects typically becomes unsatisfactory [21, 22].

Stochastic resonance (SR) can be used, as a well-known physical phenomenon, to enhance weak signals by utilizing a positive constructing role of noise [23–25]. There are already a multitude of promising applications of SR in machine fault detection and other fields [26–28]. With the development of applications of SR, researchers began to utilize SR in image processing as well [29, 30]. For example, Liu et al. [31] proposed an optimal adaptive bistable array SR-based gray-scale image restoration enhancement method. Sun et al. [32] restored pulse and high noisy images using SR. Gupta et al. [33] proposed a method for image enhancement by combining anisotropic diffusion with dynamic SR in discrete wavelet transform domain. Singh et al. [34] proposed a modified neuron model based SR approach applied for the enhancement of magnetic resonance imaging. Jha et al. [35] presented a dynamic SR-based technique in singular-value domain for contrast enhancement of dark images. Liu et al. [36] proposed a novel binary image enhancement scheme based on aperiodic SR technique. Yang et al. [37] developed an elementary theory of two-dimensional (2D) parameter-induced SR to contribute to nonlinear image processing. Chen et al. [38] proposed an algorithm of image denoising for Gaussian–Gaussian mixed noise based on SR. Fu et al. [39] presented an algorithm for enhancing the contrast of dark images based on the principle of SR in global feedback spiking network of integrate-and-fire neurons. Although the above SR-based methods can remove image noise to some extent, the image denoising method with better performance and higher efficiency is still worth of further study, especially the method for the image with strong noise. By analyzing the latest theoretical and applied research results, we find that stochastic resonance of periodic potential system has more advantages in the denoising of periodic signals than classical bitable stochastic resonance, no matter in terms of signal-to-noise ratio or processing speed [40, 41]. In addition, relevant advantages have been successfully applied to the engineering problems such as recovery of bearing fault signals under the background of strong noise [42–44]. Therefore, it is worth studying whether stochastic resonance of periodic potential system still has a leading advantage in image processing. Different from bearing fault signals, image signals cannot be expressed in periodic signals by dimensionality reduction, but always in complex aperiodic signals [31, 36]. In order to explore the application value of periodic potential stochastic resonance in the field of image denoising, this paper conducts an in-depth study.

The rest of this paper is organized as follows. In Sect. 2, all parameters of Gaussian white noise (GWN) are investigated to figure out their effect on image pollution degree. In addition, the distribution law of image noise is explored to prepare for reducing the image dimension. Then, SR of noisy aperiodic square wave signal (ASWS) is discussed to prepare for image denoising. In Sect. 3, an image denoising method by SR in a nonlinear system with a periodic potential (PSR) is proposed in further detail. Besides, adaptive SR is achieved to improve PSR

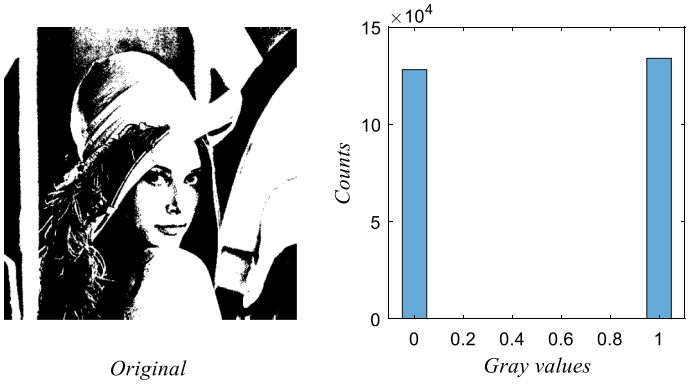

Fig. 1 Left panel. The original image is a normalized binary graph, which is used as an object of study. Right panel. The corresponding histogram of the original image

performance. In Sect. 4, three typical comparative experiments are carried out to verify the superiority of the proposed adaptive PSR method. Finally, the main conclusions are provided in the Sect. 5.

2 Preliminaries

Taking the Lena binary graph as an example which explains our algorithm simply and clearly, we denote the normalized image as $S_0(i, j)$. In addition, gray and color graphs are only additionally related to the selection of appropriate methods of image dimension reduction. As shown in Fig. 1, the original image contains only 0 and 1 pixels.

2.1 Image evaluation index

Peak signal-to-noise ratio (PSNR) is introduced to evaluate images equality because of its good evaluation ability by comparing every pixel. Two $m \times n$ monochromatic images are denoted $S(i, j)$ and $W(i, j)$, where $S(i, j)$ is the original reference image and $W(i, j)$ is the image to be evaluated. Then, their mean square error (MSE) is

$$\mathrm{MSE} = \frac{1}{m \cdot n} \sum_{i=1}^{m} \sum_{j=1}^{n} [S(i, j) - W(i, j)]^2 \tag{1}$$

PSNR is defined as

$$\mathrm{PSNR} = 10 \log_{10} \left(\frac{\mathrm{MAX}_S^2}{\mathrm{MSE}} \right) \tag{2}$$

where MAX_S represents the maximum gray level of the images. For pixel normalized images, the gray-scale range of images is within [0–1], $\mathrm{MAX}_S = 1$. Combining the above two expressions, we give the PSNR of pixel normalization image as

$$\mathrm{PSNR} = 10 \log_{10} \frac{m \cdot n}{\sum_{i=1}^{m} \sum_{j=1}^{n} [S(i, j) - W(i, j)]^2} \tag{3}$$

where m and n represent the number of images rows and columns.

Fig. 2 Image is polluted by different GWN. From left to right, the values of (μ, σ) of the GWN in the first row are (0,0.1), (0.5,0.1) and (1,0.1), and the values of PSNR are $-$ 4.3528, $-$ 15.6920 and $-$ 20.6097, respectively. In the second row, the values of (μ, σ) are (0,1), (0.5,1), (1,1), and the corresponding values of PSNR are $-$ 11.6205, -14.5271, -17.8604, respectively

2.2 Effects of different GWN parameters

To explore the effects of parameters of the Gaussian white noise (GWN), we consider the original image $S_0(i, j)$ and denote the noisy image as $S_1(i, j)$. The two parameters of GWN are the mean and the variance μ and σ, respectively. Much attention has been paid to the variance which relates to noise intensity; however, here the mean of GWN is considered as well. There are many ways to add a GWN to an image that in principle consists of adding random numbers to each pixel of the image.

As shown in Fig. 2, images with different GWN are described. Compared subplots by column, the mean values of the added GWN are the same, while their variances are different. In this case, the variance determines the image pollution degree. When the subplots are compared by row, the mean values of the GWN in images are different and the variances are the same. We can observe that not only the variance but also the mean of the GWN has a great influence on image pollution degree. In former works, little attention has been paid to analyze the influence of the mean of the GWN on image denoising.

2.3 Distribution law of image noise

As well-known, an image can be regarded as a $2D$ matrix. Do the laws of physics corresponding to a one-dimensional signal still apply to $2D$ images? This question is worth of studying. For image denoising, we want to know whether the noise distribution law in the noisy image changes or not. To clarify the confusion, we subtract $S_0(i, j)$ from $S_1(i, j)$ to obtain the noise matrix.

As shown in Fig. 3, histograms of different noise matrices are exhibited. Besides, the corresponding fitting curves are given. It can be seen that noise of the image where we have added GWN does not obey a Gaussian distribution. Actually, images usually become noisy matrices after adding noise. The noisy matrices should be reset according to the computer

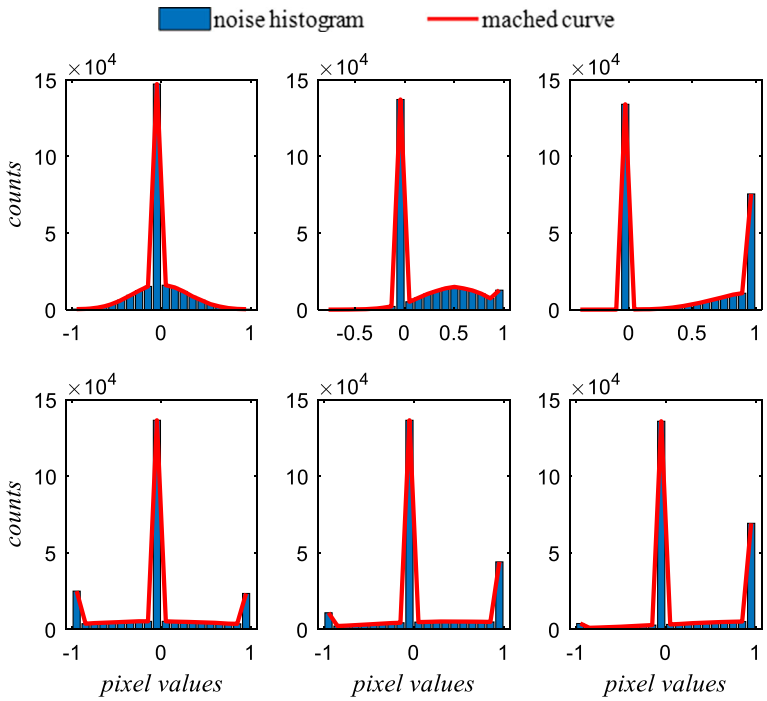

Fig. 3 Histograms of noise matrices. The subplots represent six noise matrices which are obtained by subtracting $S_0(i, j)$ by $S_1(i, j)$ of Fig. 2

imaging rules to obtain noisy images. That is, if the pixel value is greater than 1, it is reset to 1, and if is less than 0, it is reset to 0. Consequently, the noise distribution law is changed. Conversely, if the dimension of the image is reduced before computer processing after adding noise, the noise distribution law will not change. Although directly reducing image dimensions is usually operated in simulation experiments, it does not conform to the actual situation.

2.4 SR of noisy ASWS

The overdamped nonlinear system with a periodic potential can be described by the following Langevin equation

$$\frac{\mathrm{d}x}{\mathrm{d}t} = -U'(x) + S(t) + N(t) \tag{4}$$

where $S(t)$ is the input signal and $N(t)$ is the random noise. $U(x)$ is the nonlinear periodic potential function, and

$$U(x) = a\cos(bx) \quad a > 0, b > 0 \tag{5}$$

In order to denoise the image based on SR, the image needs dimension reduction. Considering the bipolarity requirement of the input signal of the nonlinear system, the one-dimensional signal obtained by dimensionality reduction is processed by dual polarization, and the obtained signal is ASWS [31, 36]. Therefore, in the simulation experiment, we take the ASWS as the input signal $S(t)$ to verify the effectiveness of PSR for image denoising.

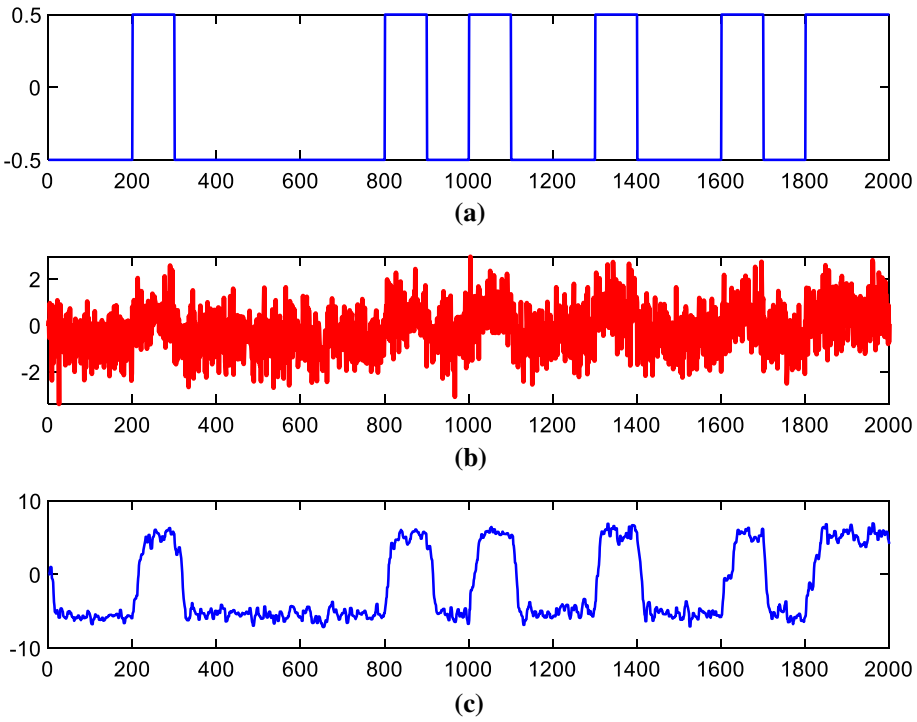

Fig. 4 SR of ASWS in the nonlinear system with a periodic potential of Eq. (4). Subplots are the original signal $L(t)$, the input signal $S(t)$ and the recovered signal $x(t)$ from top to bottom. Parameters of the periodic potential are $a = 1.68$, $b = 0.52$

In research, an ASWS denoted as $L(t)$ is generated based on a pseudo-random sequence. Then, GWN with $\mu = 0$ and $\sigma = 0.8$ is added to $L(t)$ to get $S(t)$ which is used to simulate the noisy signal. GWN which contains all frequencies and obeys a Gaussian distribution is one of the most common image noise. Therefore, it is also used when we process a one-dimensional simulation signal.

According to Eq. (4), the optimal SR can be achieved when random noise, input signal and parameters of the nonlinear system reach the optimal match. Actually, the optimal SR is hard to obtain by adjusting the noise intensity because the optimal noise cannot be predicted prior. Hence, for a certain input signal, we achieve an optimal SR by adjusting the system parameters. If not specified, we take a noisy signal $S(t)$ as the input and no longer consider the extra random noise $N(t)$.

The simulation signal $S(t)$ is substituted into Eq. (4) to observe the denoising output results. The parameters of the nonlinear system with a periodic potential is gradually changed at the same time. As shown in Fig. 4, one of the output results is presented. It can be seen that $L(t)$ is recovered from a strong noise background. Besides, the amplitude of $L(t)$ is amplified. It is believed that SR in a nonlinear system with a periodic potential can be used to recover ASWS signals from strong noise.

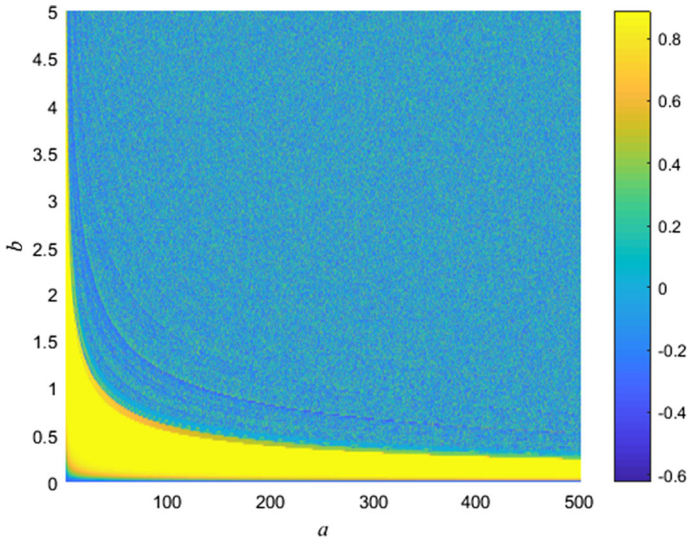

Fig. 5 Cross-correlation coefficient C_{Sx} corresponding to different system parameters a and b. The region with higher values of C_{Sx} is considered as the region where a higher probability of optimal SR might occur

The cross-correlation coefficient is introduced as an evaluation index of a one-dimensional signal, which can effectively measure the denoising performance. It is defined as

$$C_{Sx} = \frac{\mathrm{Cov}(S, x)}{\sqrt{[\mathrm{Var}(S)][\mathrm{Var}(x)]}} \tag{6}$$

where $\mathrm{Cov}(S, x)$ is the covariance of input signal S and system response x. $\mathrm{Var}(S)$ is the variance of S and $\mathrm{Var}(x)$ is the variance of x.

It is worth pointing out that PSNR can be used to evaluate images but not one-dimensional signals. Hence, C_{Sx} is used as the evaluation index when we process a one-dimensional signal.

As is well-known, parameters a and b of the periodic potential given by Eq. (5) determine the shape of the potential function. We will see that they have a great influence on our results. In addition, an input signal usually corresponds to a SR region in the nonlinear system, what means a range of system parameters corresponding to the optimal SR or nearly optimal SR. Next, we will find out the SR region of $S(t)$ in the nonlinear system with a periodic potential of Eq. (4).

Figure 5 exhibits a $2D$ plot showing the values of C_{Sx} for different pairs of a and b values of the potential. The region with large C_{Sx} can be distinguished directly. It is believed that there is a larger likelihood of achieving the optimal SR when system parameters are in this region. In practical terms, choosing the optimal parameters is an important and complicated process. Therefore, obtaining a SR region is helpful because it greatly narrows the searching range for the population initialization of the optimization algorithm.

3 Adaptive PSR image denoising

The characteristics of a signal are often submerged in a strong noise background. It is well-known that the parameters of the nonlinear system are important factors affecting the SR performance. However, optimal system parameters are hard to be obtained, which is an

optimization problem hindering wide application of SR. Fortunately, many algorithms have been proposed to solve this problem. Among them, the quantum particle swarm optimization (QPSO) algorithm is a kind of algorithm that has good ability for searching the optimal solution in the whole feasible region [45]. Therefore, the QPSO is used for the searching of optimal system parameters to achieve adaptive SR.

3.1 QPSO algorithm

The QPSO algorithm endows particles with quantum behavior, so that they can search for the optimal solution in the whole feasible region without falling into local convergence. The main optimization principle is as follows.

Firstly, the search of the range of the optimal target is defined as a D-dimensional space, in which initial population is composed of H particles. The position of the ith particle in the space is denoted as $X_i = (X_{i1}, X_{i2}, \ldots, X_{iH})^T$. In fact, the updated position vectors of each particle constitute a potential solution. Next, positions of particles are substituted into a fitness function to obtain the fitness value which can be used to evaluate the whole result. Then, the individual position of each particle is updated by tracking the individual extremum P_i and the population extremum P_g, where P_i refers to the optimal fitness position calculated from the positions experienced by a single particle. P_g refers to the optimal fitness position of all particles in the population. Finally, the optimal result is obtained when the search reaches the preset condition.

The position equation is

$$X(T) = P \pm \frac{L}{2} \ln(1/v) \tag{7}$$

where v is a random number within [0,1] and T is the number of iterations. P is the attractor, $P = uP_i + [1-u]P_g$, in which u is a random number within [0,1]. The transformation law of L is

$$L(T+1) = 2\alpha |M - X(T)|, \tag{8}$$

where M is the average value of the individual extremum corresponding to the particle position under the current iteration times $M = \frac{1}{H}\sum_{i=1}^{H} P_i$, and α is the coefficient of contraction and expansion. The position equation of the particle is obtained by substituting Eq. (8) into Eq. (7), that is,

$$X(T+1) = P \pm \alpha |M - X(T)| \ln(1/v), \tag{9}$$

The QPSO algorithm can be used to find the optimal target quickly and efficiently, which provides a basis for the realization of the adaptive image denoising.

3.2 Adaptive PSR

Here, the image denoising by SR in the system given by Eq. (4) is proposed in detail. Besides, the QPSO algorithm is utilized to obtain the optimal system parameters in order to achieve the adaptive denoising. Adaptive PSR image denoising contains the following steps:

(1) Normalize image
The noisy image to be processed are normalized firstly. The result is denoted as $I_0\ (i, j)$, in which pixel values are distributed within [0,1].

(2) Dual-polarize image
The normalized image $I_0\ (i,\ j)$ is dual-polarized. Then, the result is denoted as $I_1\ (i,\ j)$. For simplicity, $I_1\ (i,\ j)$ is obtained by subtracting 0.5 from $I_0\ (i,\ j)$. The pixel values of $I_1\ (i,\ j)$ are distributed within $[-\ 0.5,\ 0.5]$.
(3) Reduce dimensionality
$I_1\ (i,\ j)$ is reduced by the row-major order to obtain $S(k)$. Firstly, the first line of $I_1\ (i,\ j)$ is scanned, which is traversed from the first element to the last element. Then, the second line is scanned from the first element. The operation is repeated until the last element of the last line.
(4) Acquire optimal SR adaptively
Firstly, $S(k)$ is input into the system of Eq. (4). Then, the optimal system parameters are obtained with the help of the QPSO algorithm. Finally, the optimal $x(k)$ is obtained through achieving the optimal SR.
(5) Reshape image
$x(k)$ is reshaped to obtain $W\ (i,\ j)$.
(6) Binarize image
$W\ (i,\ j)$ is binarized to obtained the image $W_0\ (i,\ j)$.
(7) Statistical analysis

Steps (4), (5) and (6) are repeated for n times to get images $W_1\ (i,\ j)$,$W_2\ (i,\ j)$,..., $W_n\ (i,\ j)$. Based on Gibbs rules, the image with a large PSNR deviation is removed [46]. Then, the required image is obtained by averaging rest images.

It has to be noted that not every step is necessary in applications. Steps (1), (2) and (3) are for preprocessing. Steps (4) and (5) are the core of the algorithm. Steps (6) and (7) are for post-processing. The post-processing steps are presented to test the denoising result, which are not necessary in practical applications. In addition, if the image is scanned both in positive and transpose direction in step (3), the average of their final results will be better.

4 Experimental results and performance analysis

To evaluate the image denoising performance of the adaptive PSR, three contrast experiments are presented. Just for convenience, we report that all the experiments have been implemented on a laptop, whose main configuration is CPU: AMD Ryzen 7 2700 eight-core Processor 3.2 GHz, GPU: NVIDIA GeForce GTX1660, RAM: 6 GB.

4.1 The comparison with the adaptive BSR method

Among traditional SR-based methods, SR in a nonlinear system with a bistable potential is often used. The potential function of the bistable system is given by

$$U_0(x) = -\frac{c}{2}x^2 + \frac{d}{4}x^4 \quad c > 0, d > 0, \tag{10}$$

which corresponds to the periodic potential function $U(x)$ in Eq. (5). In the numerical experiment, we use this bistable potential into Eq. (4) in order to achieve SR, while other conditions remain unchanged to avoid interference from other factors. Hence, the adaptive SR in a bistable system (BSR) method is utilized to compare with the proposed adaptive PSR method by denoising the same image with different GWN parameters.

Figure 6 depicts denoising results of Fig. 2 by using the adaptive BSR and the adaptive PSR. The images to be denoised are polluted by having used a GWN with different parameters.

Fig. 6 Denoising results of images shown in Fig. 2 by either using the adaptive BSR method or the adaptive PSR method. From top to bottom, we show in the first row, the figures of the noisy images, in the second row, the results of the adaptive BSR, and in the third row, the results of the adaptive PSR. In the first row, (μ,σ) of GWN are (0,0.1), (0.5,0.1), (1,0.1), (0,1), (0.5,1) and (1,1), respectively. PSNR of the second row are − 3.1085, − 3.2947, − 3.5037, − 9.1659, 1.4717 and − 1.5204. PSNR of the third row are − 1.3095, 3.8906, 2.0120, − 8.7280, 3.3406 and − 0.3751

The GWN mean which has an influence on image pollution degree is considered besides the GWN variance. It can be seen that the results of the adaptive PSR method have a better visual feedback and a higher PSNR.

To further compare the adaptive BSR and the adaptive PSR under different noise intensity, Fig. 7 presents denoising results of other images by the two methods. The images to be denoised are polluted by having used a GWN with different variances. The variances of GWN added to the image are 0.5, 1, 1.5, 2, 2.5 and 3. It can be seen that the results of the adaptive PSR method have better visual feedback in all the noise background.

To objectively evaluate the image denoising performance of the two methods mentioned above, we record the PSNR of the denoised images by the two methods. The image to be processed is polluted by GWN with $\mu = 0.5$, $\sigma = 1$. Table 1 exhibits the key indexes including computation time T, the optimal PSNR and the number of convergent iterations I of the optimization algorithm. As shown in Table 1, compared with the adaptive BSR, the proposed adaptive PSR method not only improves the PSNR but also has a faster convergence speed and less computation time. In applications, if the data volume is larger, the advantage of faster convergence speed and less computation time of the adaptive PSR method will be greater.

4.2 A comparison with four other common methods

Here, we compare the adaptive PSR method with four common image denoising methods including arithmetic mean filter, geometric mean filter, median filter and Wiener filter by processing the same image with a GWN. These common methods are realized directly through calling functions in MATLAB. The arithmetic mean filter uses *imfilter*. The geometric mean filter uses $exp(imfilter(log(I))$. The median filter uses *medfilt2*. The Wiener filter uses *wiener2*. Figure 8 shows the results of all the mentioned methods.

Fig. 7 Denoising results of the same image with different GWN parameters by either using the adaptive BSR method or the adaptive PSR method. From top to bottom, we show in the first row, the figures of the noisy images, in the second row, the results of the adaptive BSR, and in the third row, the results of the adaptive PSR. The variances of GWN added in the images are 0.5, 1, 1.5, 2, 2.5 and 3, respectively, while the mean is 0.5 in all cases

Table 1 Comparison of critical indices of the adaptive BSR and the adaptive PSR

	Adaptive BSR method			Adaptive PSR method		
	Time (s)	Iterations	PSNR (dB)	Time(s)	Iterations	PSNR (dB)
1	450.3044	17	1.4696	169.9030	18	3.3816
2	455.5701	04	1.4716	165.1042	11	3.3916
3	438.0583	12	1.4726	168.7305	11	3.3406
4	444.3386	08	1.4717	166.1081	12	3.4036
5	449.0917	15	1.4726	162.9762	13	3.3876
6	450.1454	06	1.4726	168.9271	03	3.3808
7	446.2924	10	1.4726	164.9041	04	3.3786
8	451.1163	12	1.4726	171.5033	10	3.3346
9	443.8347	22	1.4726	164.1174	02	3.4016
10	445.1277	18	1.4726	171.4160	03	3.3997
11	451.3128	11	1.4726	163.5810	13	3.4006
Average	447.7445	12.2727	1.4722	167.0242	9.0909	3.3819

Table 2 exhibits the PSNR values of denoised images by different methods. The noisy image used for denoising is Lena with GWN ($\mu = 0.5$,$\sigma = 1$). From the graphs in Fig. 8 and the PSNR values in Table 2, we can see that the adaptive PSR method is better than the common image denoising methods including arithmetic mean filter, geometric mean filter, median filter, Wiener filter and BSR method.

To intuitively and objectively compare all image denoising methods mentioned above, Fig. 9 provides PSNR of different denoised images by different methods. Six different methods are compared by denoising the same noisy image, which is obtained by adding a GWN to the raw image. PSNR of noisy images before processing are also shown. As shown in

Fig. 8 Results by the proposed method and four traditional denoising methods. From left to right, the first line are the noisy image with GWN ($\mu = 0.5$,$\sigma = 1$), geometric mean filtering and arithmetic mean filtering. The second line is the median filtering, Wiener filtering and the result of the proposed method

Table 2 PSNR of denoised images by different methods

The noisy image	Geometric mean filtering	Arithmetic mean filtering	Median filtering	Wiener filtering	PSR method	BSR method
− 14.5271	− 10.1108	− 5.5229	− 4.8248	0.8791	3.4090	1.4722

the figure, adaptive PSR method has the best performance in both weak and strong noise background.

4.3 Denoising results of images with four other common noises

Image noise can be classified into different types according to its probability distribution. We have already proved the superiority of the proposed adaptive PSR method in denoising images with GWN. In order to verify the universality of the adaptive PSR, four other common types of noise, we perform experiments using other types of noise to simulate image noise including gamma noise, uniform noise, Rayleigh noise and exponential noise. The denoised images are shown in Fig. 10.

Table 3 presents the PSNR values corresponding to subplots of Fig. 10. From the graphs in Fig. 10 and the PSNR values in Table 3, it can be seen that the proposed adaptive PSR method can also remove other types of image noise effectively.

In the above comparative experiments, Lena is used as the research object to simulate image denoising under different noise intensity backgrounds, where the denoising effects of PSR, BSR and four common traditional methods are, respectively, compared. At the same time, PSR method is verified to denoise images with different types of noise. In order to fully validate the productivity of the proposed adaptive PSR method, we select another new

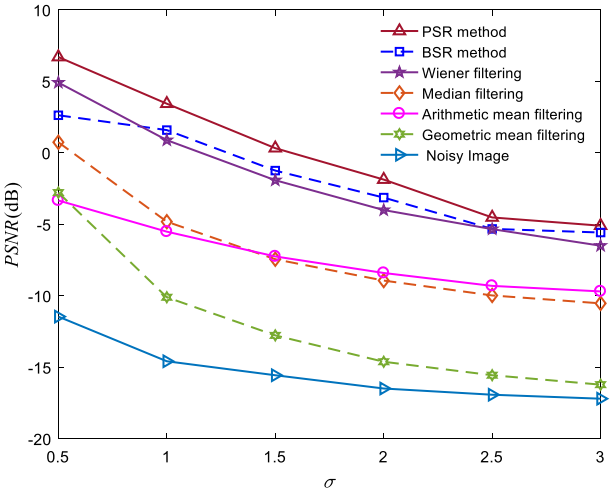

Fig. 9 PSNR of the noisy image denoised by different methods. The parameter σ represents the variance of the GWN

Fig. 10 Denoised results of the image polluted by different types of noise including gamma noise, uniform noise, Rayleigh noise and exponential noise. The first row represents noisy images, while the second row represents the corresponding denoised results

research object, Cameraman, to carry out a new set of comparative experiments, and the results are as follows.

4.4 The comparison with the adaptive BSR method for another image

Figure 11 depicts denoising results of noisy images of Cameraman by using the adaptive BSR and the adaptive PSR. The images to be denoised are polluted by having used a GWN with different parameters, including the GWN mean and variance. It can be seen that the results of the adaptive PSR method have a better visual feedback and a higher PSNR.

Table 3 Value of the PSNR for different noise images before and after being processed by the adaptive PSR

	Gamma noise	Uniform noise	Rayleigh noise	Exponential noise
Before	− 21.6373	− 21.6225	− 21.8751	-21.6391
After	0.4407	6.3367	5.6098	4.2133

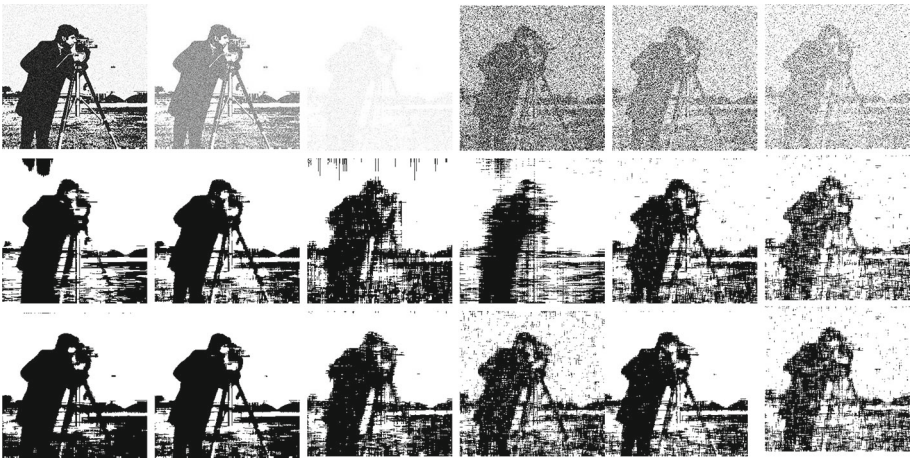

Fig. 11 Denoising results by either using the adaptive BSR method or the adaptive PSR method. From top to bottom, we show in the first row, the figures of the noisy images, in the second row, the results of the adaptive BSR, and in the third row, the results of the adaptive PSR. In the first row, (μ,σ) of GWN are (0,0.1), (0.5,0.1), (1,0.1), (0,1), (0.5,1) and (1,1), respectively. PSNR of the first row are 9.8051, − 11.0134, − 16.6968 − 6.9624, − 11.4650 and − 12.6377. PSNR of the second row are − 3.9679, 3.6910, − 1.7225, − 6.4821, 1.3481 and − 5.8723. PSNR of the third row are − 1.1249, 7.4676, 1.3014, − 3.0563, 3.2001 and − 0.8666

To further compare the adaptive BSR and the adaptive PSR under different noise intensity, Fig. 12 presents denoising results of other images by the two methods. The images to be denoised are polluted by using a GWN with different variances. The variances of GWN added to the image are 0.5, 1, 1.5, 2, 2.5 and 3. It can be seen that the results of the adaptive PSR method have better visual feedback in all the noise background.

To objectively evaluate the image denoising performance of the two methods mentioned above, we record the PSNR of the denoised images by the two methods. The image to be processed is polluted by GWN with $\mu = 0.5$, $\sigma = 1$. Table 4 lists the key indexes including computation time, the optimal PSNR and the number of convergent iterations of the optimization algorithm. As shown in Table 4, compared with the adaptive BSR, the proposed adaptive PSR method not only improves the PSNR but also has a faster convergence speed and less computation time. In applications, if the data volume is larger, the advantage of faster convergence speed and less computation time of the adaptive PSR method will be greater.

4.5 A comparison for another image with four other common methods

As shown in Fig. 13, we compare the adaptive PSR method with four common image denoising methods including arithmetic mean filter, geometric mean filter, median filter and Wiener filter by processing the same Cameraman with a GWN. These common methods are realized directly through calling functions in MATLAB. The arithmetic mean filter uses *imfilter*. The

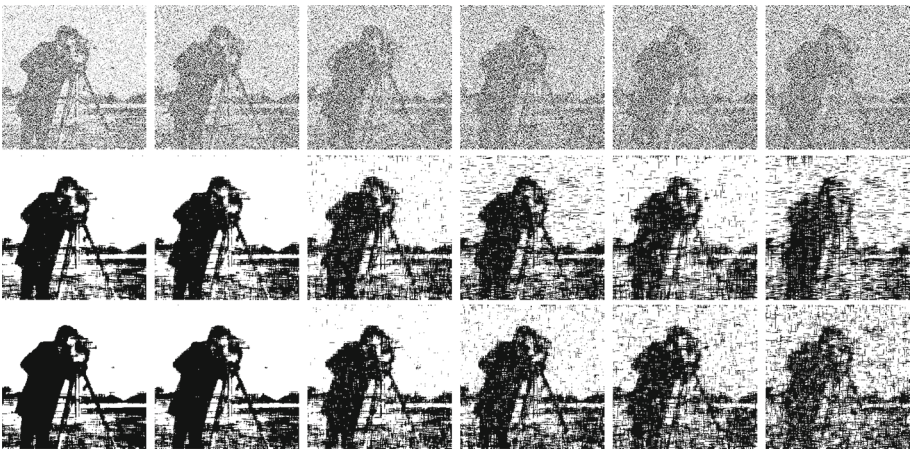

Fig. 12 Denoising results of the same Cameraman with different GWN parameters by either using the adaptive BSR method or the adaptive PSR method. From top to bottom, we show in the first row, the figures of the noisy images, in the second row, the results of the adaptive BSR, and in the third row, the results of the adaptive PSR. The variances of GWN added in the images are 0.5, 1, 1.5, 2, 2.5 and 3, respectively, while the mean is 0.5 in all cases. PSNR of the first row are − 10.0846, − 11.4650, − 13.5891, − 14.5666, − 15.2292 and − 15.6377. PSNR of the second row are 3.9679, 1.3910, 1.1450, − 1.5592, − 4.2518 and − 4.8723. PSNR of the third row are 5.3987, 3.2676, 2.2761, − 0.6563, − 3.2001 and − 4.2518

Table 4 Comparison of critical indices of the adaptive BSR and the adaptive PSR

	Adaptive BSR method			Adaptive PSR method		
	Time (s)	Iterations	PSNR (dB)	Time (s)	Iterations	PSNR (dB)
1	111.1682	14	1.3696	47.9115	10	3.2816
2	115.2553	19	1.3716	46.9755	06	3.2916
3	112.8278	11	1.3726	46.2305	14	3.2406
4	124.9596	16	1.3717	48.1831	12	3.2036
5	113.9519	10	1.3726	49.1003	04	3.2876
6	126.6635	10	1.3726	47.5027	09	3.2808
7	136.4892	12	1.3726	46.6725	10	3.2786
8	117.2318	06	1.3726	46.6262	07	3.2346
9	134.7117	11	1.3726	50.9565	06	3.2016
10	119.0295	14	1.3726	46.2405	13	3.2997
11	115.7567	13	1.3726	48.1831	11	3.2006
Average	123.6363	12.2727	1.3722	47.6893	9.2727	3.2546

geometric mean filter uses $exp(imfilter(log(I))$. The median filter uses *medfilt2*. The Wiener filter uses *wiener2*. Figure 13 shows the results of all the mentioned methods.

Table 5 exhibits the PSNR values of denoised images by different methods. The noisy image used for denoising is Cameraman with GWN ($\mu = 0.5, \sigma = 1$). From the graphs in Fig. 13 and the PSNR values in Table 5, we can see that the adaptive PSR method is better than the common image denoising methods including arithmetic mean filter, geometric mean filter, median filter, Wiener filter and BSR method.

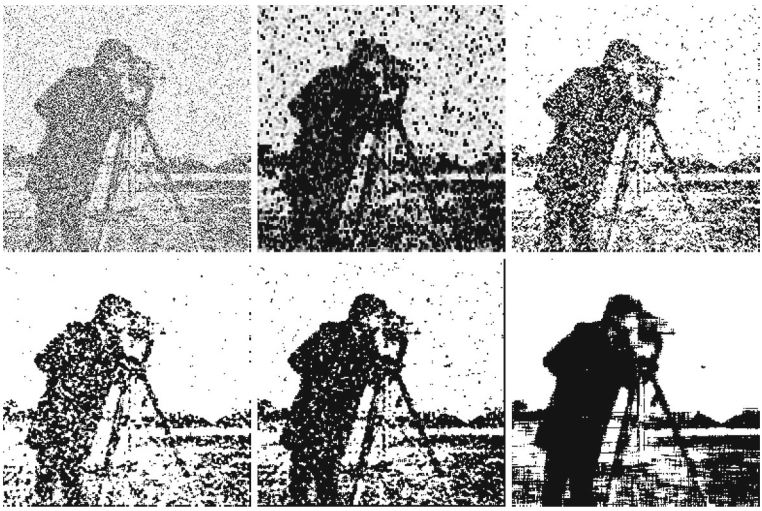

Fig. 13 Results by the proposed method and four traditional denoising methods. From left to right, the first line are the noisy image with GWN ($\mu = 0.5$,$\sigma = 1$), geometric mean filtering and arithmetic mean filtering. The second line is the median filtering, Wiener filtering and the result of the proposed method

Table 5 PSNR of denoised images by different methods

The noisy image	Geometric mean filtering	Arithmetic mean filtering	Median filtering	Wiener filtering	PSR method	BSR method
− 11.4650	− 8.7361	− 6.9398	− 4.7954	− 0.4820	3.2786	1.3910

To intuitively and objectively compare all image denoising methods mentioned above, Fig. 14 provides PSNR of different denoised images by different methods. Six different methods are compared by denoising the same noisy image, which is obtained by adding a GWN to the raw image. PSNR of noisy images before processing are also shown. As shown in the figure, adaptive PSR method has the best performance in both weak and strong noise background.

4.6 Denoising results of images with four other common noises

Image noise can be classified into different types according to its probability distribution. We have already proved the superiority of the proposed adaptive PSR method in denoising images with GWN. In order to verify the universality of the adaptive PSR, four other common types of noise, we perform experiments using other types of noise to simulate image noise including gamma noise, uniform noise, Rayleigh noise and exponential noise. The denoised images are shown in Fig. 15.

Table 6 presents the PSNR values corresponding to subplots of Fig. 15. From the graphs in Fig. 15 and the PSNR values in Table 6, it can be seen that the proposed adaptive PSR method can also remove other types of image noise effectively.

As shown above, we reproduce the comparison experiment with another image, i.e., Cameraman. As shown in the above figures and tables, the new object has same experimental

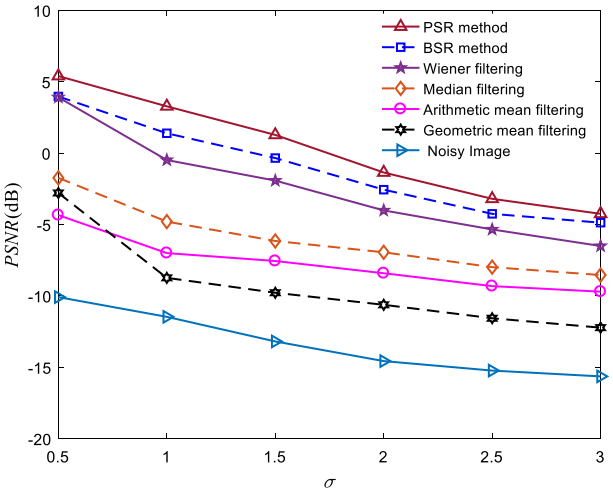

Fig. 14 PSNR of the noisy image denoised by different methods. The parameter σ represents the variance of the GWN

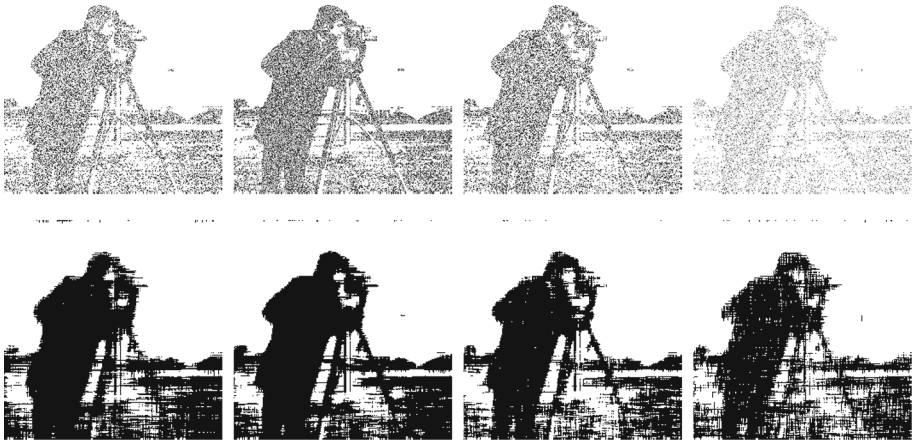

Fig. 15 Denoised results of the image polluted by different types of noise including gamma noise, uniform noise, Rayleigh noise and exponential noise. The first row represents noisy images, while the second row represents the corresponding denoised results

comparison results with Lena. In fact, adaptive PSR has no special requirements for handling objects. In other words, adaptive PSR method has universality to a certain extent.

5 Conclusion

This work proposes an adaptive PSR image denoising method based on the use of the constructive role of noise played by a simple nonlinear system with a periodic potential. Further, the method achieves adaptive denoising by utilizing the QPSO algorithm. Through numerical experiments, the superiority of the proposed adaptive PSR method is verified. It can be concluded that the method has a stable performance in both weak and strong noise background.

Table 6 Value of the PSNR for different noise images before and after being processed by the adaptive PSR

	Gamma noise	Uniform noise	Rayleigh noise	Exponential noise
Before	− 15.9812	− 15.8262	− 15.6042	− 16.0144
After	0.1712	3.9452	4.5073	0.6898

In addition, all the GWN parameters including variance and mean are considered to clarify their roles on polluted images. It is found that the mean of GWN also has a great influence on image pollution degree besides the variance. The noise of images where a GWN has been added are explored as well. It is known that the noise no longer obeys a Gaussian distribution because images should be reset after adding noise. That is, image dimension should not be reduced directly after adding noise. Besides, noise in a one-dimensional signal is not in a GWN form even if the signal is obtained by reducing the image after having added the GWN.

To sum up, this study not only provides an adaptive PSR denoising method with a higher efficiency and a better performance for images with a strong noise, but also presents some new insights of image noise. The paper may also provide some ideas for other types of image processing.

Acknowledgements This work is supported by the National Natural Science Foundation of China (Grant No. 12072362), the Graduate Research and Innovation Projects of Jiangsu Province, the Priority Academic Program Development of Jiangsu Higher Education Institutions and by the Spanish State Research Agency (AEI) and the European Regional Development Fund (ERDF, EU) under Project No. PID2019-105554GB-I00.

References

1. B. Goyal, A. Dogra, S. Agrawal, B.S. Sohi, A. Sharma, Inf. Fusion **55**, 220–244 (2020)
2. Y. Quan, Y. Chen, Y. Shao, H. Teng, Y. Xu, H. Ji, Pattern Recognit. **111**, 107639 (2021)
3. J. Xiao, R. Zhao, K.M. Lam, Signal Process. Image Commun. **96**, 116299 (2021)
4. B. Ghanbari, A. Atangana, Phys. A **542**, 123516 (2020)
5. C.S. Asha, M. Singh, S. Suresh, S. Lal, Remote Sens. Appl. **20**, 100415 (2020)
6. C. Jaspin Jeba Sheela, G. Suganthi, Biomed. Signal Proces. **55**, 101657 (2020)
7. R. Vidhya, M. Brindha, N. Ammasai Gounden, Chin. J. Phys. **62**, 26–42 (2019)
8. H. Li, C.Y. Suen, Pattern Recognit. **49**, 237–248 (2016)
9. C. Wu, X. Ma, W. Wang, J. Intell. Fuzzy Syst. **37**(4), 4425–4429 (2019)
10. A. M. John, K. Khanna, R. R. Prasad and L. G. Pillai, *Fourth International Conference on I-SMAC* (IoT in Social, Mobile, Analytics and Cloud), Palladam, India, 2020, pp. 389–397
11. A. Miri, S. Sharifian, S. Rashidi, M. Ghods, Optik **156**, 938–948 (2018)
12. M. Saeedzarandi, H. Nezamabadi-pour, S. Saryazdi, J. AI Data Min. **8**(2), 289–301 (2020)
13. M. Lebrun, Image Process. **2**, 175–213 (2012)
14. M.W. Shi, F. Zhang, S.W. Wang, C.M. Zhang, X.M. Li, Comput. Vis. Image Underst. **206**, 103173 (2021)
15. K. Zhang, W. Zuo, Y. Chen, D. Meng, L. Zhang, IEEE Trans. Image Process. **26**(7), 3142–3155 (2017)
16. C. Tian, Y. Xu, W. Zuo, Neural Netw. **121**, 461–473 (2020)
17. S. Annam, A. Singla, *Sixth International Conference on Parallel, Distributed and Grid Computing*, 2020, pp. 318–323
18. A. Javeed, T. Shah, Chin. J. Phys. **66**, 645–659 (2020)
19. Q. Wang, J. Ma, S.Y. Yu, L.Y. Tan, Chaos Soliton. Fract. **131**, 109463 (2020)
20. H. Zhang, J. Yu, Y. Ma, Z. Pan, J. Zhao, Complexity **2020**, 8843950 (2020)
21. C. Ma, J. Ao, Int. J. Elec. Eng. Educ. (2020). https://doi.org/10.1177/0020720920940613
22. S. Anuranjeeta, N. Sharma, M. Sharma, K.K. Singh, Shukla. Int. J. Med. Eng. Inf. **12**(2), 180–193 (2020)
23. C. Wu, Z. Wang, J. Yang, D. Huang, M.A. Sanjuán, Eur. Phys. J. Plus **135**(1), 130 (2020)
24. J. Yang, M.A.F. Sanjuán, P. Chen, H. Liu, Eur. Phys. J. Plus **132**, 432 (2017)
25. R. Liu, Y. Kang, Y. Fu, G. Chen, Int. J. Bifurcat. Chaos **29**(08), 1950108 (2019)
26. Z. Qiao, Y. Lei, N. Li, Mech. Syst. Signal Process. **122**, 502–536 (2019)

27. S. Lu, Q. He, J. Wang, Mech. Syst. Signal Process. **116**, 230–260 (2019)
28. T. Abdeljawad, S. Banerjee, G.C. Wu, Optik **218**, 163698 (2020)
29. X. Feng, H. Liu, N. Huang, Z. Wang, Y. Zhang, Sci. Rep. **9**(1), 1–9 (2019)
30. R. Chouhan, R.K. Jha, P. Biswas, IET Image Process. **7**(22), 174–184 (2013)
31. J. Liu, H. Hu, Y. Wang, Phys. Lett. A **383**(13), 1457–1465 (2019)
32. Q. Sun, H. Liu, N. Huang, Z. Wang, J. Han, S. Li, Sci. Rep. **5**, 1–6 (2015)
33. N. Gupta, R.K. Jha, J. Electron. Imaging **25**(2), 023017 (2016)
34. M. Singh, A. Verma, N. Sharma, Biocybern. Biomed. Eng. **37**(1), 124–134 (2017)
35. R.K. Jha, R. Chouhan, Signal Image Video Process. **8**(2), 339–347 (2014)
36. J. Liu, Z. Li, IET Image Process. **9**(5), 1033–1038 (2015)
37. Y. Yang, Z. Jiang, B. Xu, D. Repperger, J. Phys. A, Math. Theor. **42**(14), 145207 (2009)
38. J. Chen, Y. Zhang, J. Song, *Eleventh International Conference on Digital Image Processing*, Guangzhou, China, 2019, pp. 1117904
39. Y.X. Fu, Y.M. Kang, G.R. Chen, Front. Comput. Neurosci. **14**(24), 1–11 (2020)
40. J. Zhang, D. Huang, J. Yang, H. Liu, X. Liu, J. Mech. Sci. Technol. **31**(10), 4599–4610 (2017)
41. K. Liu, Y. Jin, Phys. A **392**(21), 5283–5288 (2013)
42. Z. Li, X. Liu, T. He, Y. Shan, IEEE Access **7**, 141633–141647 (2019)
43. J. Liu, Z. Qiao, X. Ding, B. Hu, C. Zhang, Chaos Soliton. Fract. **146**, 110845 (2021)
44. T. Liu, S. Banerjee, H. Yan, J. Mou, Eur. Phys. J. Plus **136**(5), 1–17 (2021)
45. Z.J. Wang, Z.H. Zhan, S. Kwong, H. Jin, J. Zhang, IEEE Trans. Cybern. **51**, 1–24 (2020)
46. M. Billio, R. Casarin, A. Osuntuyi, Comput. Stat. Data Anal. **100**, 37–57 (2016)